A diagrammatic approach for a clean double-barrier ferromagnetic Josephson junction

2008 J. Phys. A: Math. Theor. 41 455301

(http://iopscience.iop.org/1751-8121/41/45/455301)

IOP PUBLISHING JOURNAL OF PHYSICS A: MATHEMATICAL AND THEORETICAL

J. Phys. A: Math. Theor. **41** (2008) 455301 (19pp) doi:10.1088/1751-8113/41/45/455301

A diagrammatic approach for a clean double-barrier ferromagnetic Josephson junction

V Paltoglou, I Margaris and N Flytzanis

Department of Physics, University of Crete, PO Box 2208, 71003 Heraklion, Greece

Received 17 April 2008, in final form 5 September 2008
Published 8 October 2008
Online at stacks.iop.org/JPhysA/41/455301

Abstract

We consider a double-barrier superconductor/ferromagnet/superconductor (S/I/F/I/S) ballistic junction with thin insulating layers at the interfaces. Using a diagrammatic approach we obtain the Andreev spectrum and the supercurrent in terms of the S/F interface scattering amplitudes. We use the rules devised for the summation of the multiple scattering diagrams. We especially concentrate on the strong interface scattering and consider the evolution of the supercurrent. We observe that in this case the normal spin-up and spin-down electron (hole) resonances determine well the supercurrent, except near the strong peaks, where the Andreev diagrams are also important. At lower $Z \approx 2$ values we also need to keep other closed loops. We consider both the one- and three-dimensional cases. We also consider the case of strong band misfit. The current–phase relation shows a broad range of behavior with 0–π regions and transitions where higher harmonics in the phase contribute dominantly.

PACS numbers: 74.45+c, 74.78.Fk, 73.23.Ad

(Some figures in this article are in colour only in the electronic version)

1. Introduction

In superconductor/normal/superconductor (S/N/S) Josephson junctions at low temperatures the flow happens by means of the Andreev reflection [1–3] mechanism, where an electron incident from the metal side and energy in the superconducting gap, is reflected from the NS interface as a hole with the opposite spin, while at the same time a pair is transmitted in the superconductor. At low temperatures they appear as *current-carrying bound states* [4] of a multiple reflected electron–hole pair inside the intermediate region, forming coherent pairs even though no attractive interaction exists between them. During the Andreev process the electron–hole pairs retain information on the superconducting condensate and they mediate the superconducting phase coherence across the junction even when we use a stepwise gap function amplitude. This is a reasonable approximation in the case of weak transparency

due to strong interface barriers, which will be the case in this work. Otherwise one must be confronted with the task of solving self-consistently for the gap function [5]. The region in the normal part over which the coherence is carried depends on the scattering properties in the junction, but is also an inherent property of the Andreev process. Thus, the momentum mismatch at energy E of the electron–hole pair leads to the loss of coherence and the phase shift due to branch crossing processes determine the bound states [1, 3, 6, 7], which are called Andreev-bound states (ABS).

In the case of a ferromagnet in contact with an s-superconductor, the electrons and reflected holes in the ferromagnet, due to the opposite spins, get a Zeemann splitting from the exchange field E_{ex} ($E_{\mathrm{ex}} \gg \Delta$), so that we have correlated pairs with non-zero total momentum (even at the Fermi level) and a significant decoherence in the electron and retroreflected hole at the FS interfaces [8–14]. The proximity effect is limited near the surface for singlet superconductivity. In general one can consider two types of S/F/S junctions: one with low concentration of impurities, where the transport can be considered ballistic and coherent and the second case of strong impurity scattering, so that the transport is diffusive. While the second case is more usual, with the development of film preparation techniques [15–17], the ballistic regime is also accessible to experimental work. For S/F/S junctions extensive work has been done in both the clean limit [5, 18, 19] and diffusive limit [12] using the quasiclassical theory [20, 21], and in the quasiballistic limit [22] using the Eilenberger equations. Experimentally both weak [23–26] and strong [27–30] ferromagnets were studied.

In the S/F/S hybrid junction, an interesting experimental observation is the π-junction behavior which was predicted long time ago for the case of paramagnetic impurities [8] and observed experimentally [24, 27, 31, 32]. The 0–π transition has also been studied theoretically in the clean [19, 33–35] and diffusive [10, 36, 37] limit. Well-characterized interfaces [15] between ferromagnet and superconductors provide the possibility of studying the coexistence and competition of ferromagnetism and superconductivity [11, 12], spin-dependent transport properties [38] and magnetosemiconductor junctions [39].

For clean interfaces and weak ferromagnets the basic mechanism of the bound states involves two Andreev reflections, at one interface from electron to hole and vice versa at the other interface. Several analytic approximations can be obtained for the discrete Andreev spectrum, using the Andreev approximation [3, 11, 12, 34, 40] for a single ferromagnetic layer if we neglect band misfit and normal scattering between the layers. The discrete Andreev spectrum at low temperatures gives the main contribution to the supercurrent [6, 41–43].

For the low-transparency junction it is reasonable to assume that the normal scattering processes depending on the quality of the interface and band misfit are equally important [44]. Thus several studies considered the effect of double barriers for metal [45–49], insulator [51], ferromagnet [12, 19, 40, 52, 53] and superconductor [44, 54] intermediate layers. In general, the supercurrent dependence on the various interface scattering amplitudes is obtained via the scattering matrix approach [3, 53, 55, 56]. For the multiple scattering processes we will use a diagrammatic procedure for the determination of the Andreev spectrum and supercurrent, which can be simplified in a systematic way by focusing on the dominant paths [57, 58].

In this paper we consider low-transparency barriers and clean layers, with relatively strong ferromagnets. Since the quasiclassical treatment in these limits is not sufficient, we use the solutions of Bogoliubov–de Gennes equations. We do not consider the effects of diffusive scattering. On the other hand we concentrate on equally important factors such as strong spin polarization, Fermi wave vector mismatch and interfacial resistance, taking into account the refinement of new experimental techniques in materials growth. In this case, there is a strong interplay between Andreev-bound states and normal resonances of electrons or holes of either spin in the double-barrier IFI structure [12, 19, 52], when resonances cross the Fermi level.

In the case of a single-channel (1D) transport the resonances drive $0 \rightarrow \pi$ (or vice versa) transitions and the critical current variation with ferromagnetic width, $I_c(d)$, is highly peaked [52] and quite surprising. At relatively high transparencies these transitions disappear, due to the broadening of the resonances, except for transitions that one expects at $Z = 0$. Here we will extend these results to planar junctions (3D problem) and in particular the situation where we have the coincidence of spin-up and spin-down resonances. We see that in this case, for the single-channel transport, we obtain greatly enhanced transport, that approaches that of the resonant *SINIS* structure [52]. We will discuss the conditions for the spin-up and spin-down resonances coincidence in the planar junction. For this case the diagrammatic approach will guide us to understand the structure of resonances and decide which approximations are suitable for a selective summation of the important scattering processes, as determined by the strength of the various interface scattering amplitudes. In section 2 we present the model for the hybrid junction, we summarize the results of the diagrammatic approach that includes all the closed scattering paths for the S/I/F/I/S junction and derive an expression for the condition for the Andreev spectrum. The calculation of the current is presented in section 3 for a single-channel transport, which is also extended to planar junctions. In the final section we summarize our results.

2. The $S_L/I_L/F/I_R/S_R$ model

We consider a clean hybrid junction consisting of two bulk superconductors and an intermediate ferromagnet of thickness d, with strong interface scattering. Thus we can assume a simple step-like spatial dependence of the order parameter, with $\Delta(z) = \Delta_\alpha(T)\, e^{i\phi_\alpha}$ with $\alpha = L, R$ for the left ($z < 0$) and right ($z > d$) superconductors and vanishing elsewhere ($\Delta = 0$ for $0 < z < d$). The temperature dependence of the bulk superconducting gap is $\Delta_\alpha(T) = \Delta_{0,\alpha} \tanh\left(1.74\sqrt{T_{c,\alpha}/T - 1}\right)$. The ferromagnetic layer is described with the effective exchange energies E_{ex}. The exchange field shifts the Fermi levels of the two-spin subbands and also causes ordinary reflections at the SF interfaces due to the Fermi energy mismatch. Except the exchange field misfit, the case of band parameter misfit between the ferromagnet and superconductor is included.

Due to the piecewise constant gap and exchange energy, the scattering states are characterized by wave vectors. Due to the homogeneity parallel to the junction plane, the parallel wave vector ($\vec{k}_\parallel$) is conserved, so that we have to solve for the z dependence of the wavefunction. Thus in the absence of spin-flip processes the two-spin channels are decoupled for each set of solutions ($u_\sigma(z)$, $v_{-\sigma}(z)$) and the BdG equations are

$$\begin{pmatrix} H_0 + V_\sigma(z) & \Delta(z) \\ \Delta^*(z) & -[H_0 + V_{-\sigma}(z)] \end{pmatrix} \begin{pmatrix} u_\sigma(z) \\ v_{-\sigma}(z) \end{pmatrix} = E \begin{pmatrix} u_\sigma(z) \\ v_{-\sigma}(z) \end{pmatrix}. \tag{1}$$

The diagonal terms of the BdG equations are written in the effective mass approximation

$$H_0 = -\hbar^2 \frac{\partial}{\partial z} \frac{1}{2m(z)} \frac{\partial}{\partial z} + \frac{\hbar^2 k_\parallel^2}{2m(z)} + V(z). \tag{2}$$

In the calculations we consider only uniform effective electron mass, equal to m_S in the superconducting and ferromagnetic layers. All wave vectors will be normalized to the Fermi wave vector $k_F = \left(\frac{2m_S E_F}{\hbar^2}\right)^{1/2}$, with E_F being the uniform Fermi energy. Length is normalized to the coherence length ξ_0. Thus in the exponentials the dimensionless parameter $\kappa = k_F \xi_0 = \frac{2}{\pi} \frac{E_F}{\Delta_0}$ must be introduced.

In (2) $V(z) = W(z) + U(z) - \mu$ is the total potential, where $U(z)$ and μ are the electrostatic and the chemical potential, respectively, which constant values in each layer of

the junction. The scattering at the S/F interface insulating layers are modeled by delta-barrier potentials of the form $W(z) = Z_\alpha \delta(z - z_\alpha)$ for the two S/F interfaces at $z_L = 0, z_R = d$, normalized to $Z_F = E_F/k_F$, where the Fermi wave vector and energy are chosen in the left superconductor. Here we consider only the case where the left and right superconductors are the same $\Delta_{L0} = \Delta_{R0}$ and also the interface scattering potential $Z_R = Z_L$. Since we examine the behavior of the junction in the ballistic limit no other scattering processes take place in the bulk of the layers due to disorder or spin-flip processes.

The BdG equations are easily solved in each layer and then matched at the interfaces. For the superconducting regions ($\alpha = L, R$) the solutions are

$$\psi_\alpha^{\pm e}(z) = \exp[\pm \mathrm{i}\kappa k_{\alpha,e} z] \begin{pmatrix} u_\alpha \, \mathrm{e}^{+\mathrm{i}\phi_\alpha/2} \\ v_\alpha \, \mathrm{e}^{-\mathrm{i}\phi_\alpha/2} \end{pmatrix}, \tag{3}$$

$$\psi_\alpha^{\pm h}(z) = \exp[\mp \mathrm{i}\kappa k_{\alpha,h} z] \begin{pmatrix} v_\alpha \, \mathrm{e}^{+\mathrm{i}\phi_\alpha/2} \\ u_\alpha \, \mathrm{e}^{-\mathrm{i}\phi_\alpha/2} \end{pmatrix}. \tag{4}$$

Here $\pm e(h)$ indicates the electron(hole)-like quasiparticle moving to the right(+) or left(−), $u_\alpha = \sqrt{(1 + \Omega_\alpha/E)/2}$ and $v_\alpha = \sqrt{(1 - \Omega_\alpha/E)/2}$ are the BCS amplitudes and $\Omega_\alpha = \sqrt{E^2 - \Delta_\alpha^2}$. The normalized wave vectors are

$$k_{\alpha,p} = \left[1 - k_\parallel^2 \pm \mathrm{sign}(E) \frac{\Omega_\alpha}{E_F} \right]^{1/2}. \tag{5}$$

In the ferromagnetic region,

$$\psi^{\pm e}(z) = \exp[\pm \mathrm{i}\kappa q_{e,\sigma} z] \begin{pmatrix} 1 \\ 0 \end{pmatrix}, \qquad \psi^{\pm h}(z) = \exp[\mp \mathrm{i}\kappa q_{h,-\sigma} z] \begin{pmatrix} 0 \\ 1 \end{pmatrix}, \tag{6}$$

with the normalized wave vectors in each layer

$$q_{e,\sigma} = r_q \left[1 - k_\parallel^2 + \left(\frac{E}{r_E E_F} + \sigma \eta \right) \right]^{1/2}, \tag{7}$$

$$q_{h,-\sigma} = r_q \left[1 - k_\parallel^2 - \left(\frac{E}{r_E E_F} + \sigma \eta \right) \right]^{1/2}, \tag{8}$$

where r_q is the Fermi wave vector in the ferromagnet normalized to that in the left superconductor, r_E is the Fermi energy ratio (taken from the bottom of the conduction band) and we define the dimensionless exchange parameter $\eta = \frac{E_{\mathrm{ex}}}{r_E E_F}$.

A property of interest is the spectrum of Andreev levels and their contribution to the supercurrent. The spectrum is obtained by summing all the closed loops following a set of well-defined rules [53]. One can obtain a closed form by summing all multiple scatterings that lead to closed loops, reducing the problem to a finite number of basic processes. This can be expressed in a diagramatic approach for finding the analytic expression, in the form $\Gamma(E) = 0$, using the SF interface scattering amplitudes, which include normal ($e \to e, h \to h$) and Andreev ($e \to h, h \to e$) processes. The corresponding amplitudes are given in the appendix for incidence from the ferromagnet side and the superconductor side. The systematic procedure to be followed also allows us to introduce several possible limits in a direct way, as will be demonstrated in the following sections. Γ also arises in the form of a determinant in the denominator of the scattering matrix and Green's function and includes only a few basic terms with closed diagrams, which when expanded give all the possible closed paths.

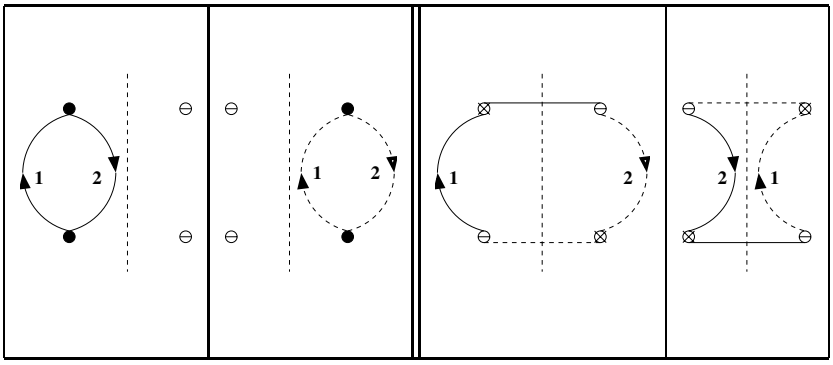

Figure 1. Lowest-order diagrams, x_1, x_2, x_3 and x_4, with two scattering events at S/F interfaces.

2.1. The Andreev spectrum condition

All closed loops (in Γ) correspond to processes that involve two or four reflections at the SF interfaces. The loops with two scattering events are shown in figure 1, where we consider both electron (continuous lines) and hole (dashed lines) propagation. At each interface we introduce two vertices that describe scattering events of incident electrons and holes correspondingly. The vertices on the same interface are connected via the Andreev process. To denote that a vertex is Andreev reflection active we use the symbol $\bigotimes$. In the first (second) diagram we have normal electron (hole) reflections with inactive vertices at the hole (electron) side. Their corresponding contributions are labeled x_1 and x_2. The other two diagrams in figure 1 correspond to Andreev reflections at the two interfaces and give the contributions labeled x_3 and x_4. This is demonstrated by the horizontal lines that connect the electron and hole paths to the left and right of the vertical dashed line.

In terms of the interface scattering amplitudes $a_{p\alpha}$, $b_{p\alpha}$ defined in the appendix for an S/F interface, the contributions to the amplitude for the different processes are

$$x_1 = \tilde{b}_{\mathrm{eL}}\tilde{b}_{\mathrm{eR}}, \qquad x_2 = \tilde{b}_{\mathrm{hL}}\tilde{b}_{\mathrm{hR}}, \tag{9}$$

$$x_3 = \tilde{a}_{\mathrm{eR}}\tilde{a}_{\mathrm{hL}}, \qquad x_4 = \tilde{a}_{\mathrm{hR}}\tilde{a}_{\mathrm{eL}}, \tag{10}$$

with the tilded scattering amplitudes given by the corresponding untilded amplitudes, like $a_{p\alpha}$, multiplied by the preceding propagation factor, i.e. for the $p = e, h$ particle before striking the α interface, so that for example $\tilde{a}_{\mathrm{eR}} = a_{\mathrm{eR}}\, \mathrm{e}^{\mathrm{i}q_e d}$. Thus the propagation factors are $\mathrm{e}^{2\mathrm{i}S_e}(\mathrm{e}^{-2\mathrm{i}S_h})$ for $x_1(x_2)$ correspondingly and for x_3 and x_4, with $S_e(S_h)$ the electron (hole) propagation phases. The terms x_1 and x_2 that correspond to normal reflections have no ϕ-dependence, while in the Andreev processes $x_3(x_4)$ the phase enters into $\mathrm{e}^{\mathrm{i}\phi}(\mathrm{e}^{-\mathrm{i}\phi})$ correspondingly, with $\phi = \phi_R - \phi_L$ the phase difference between the two superconductors.

The summation of all the closed loops gives

$$\Gamma = 1 - \gamma = 1 - [x_1 + x_2 + x_3 + x_4 - (x_1x_2 + x_3x_4 - x_5 - x_6)] \equiv \gamma_2 + \gamma_4, \tag{11}$$

where the processes in γ_2 (two scattering events) are shown in figure 1 and in γ_4 (four scattering events) the terms x_1x_2, x_3x_4, x_5, x_6 are shown in figure 2, with the contribution of the last two diagrams given by

$$x_5 = \tilde{b}_{\mathrm{eR}}\tilde{a}_{\mathrm{eL}}\tilde{b}_{\mathrm{hR}}\tilde{a}_{\mathrm{hL}}, \qquad x_6 = \tilde{a}_{\mathrm{eR}}\tilde{b}_{\mathrm{hL}}\tilde{a}_{\mathrm{hR}}\tilde{b}_{\mathrm{eL}}. \tag{12}$$

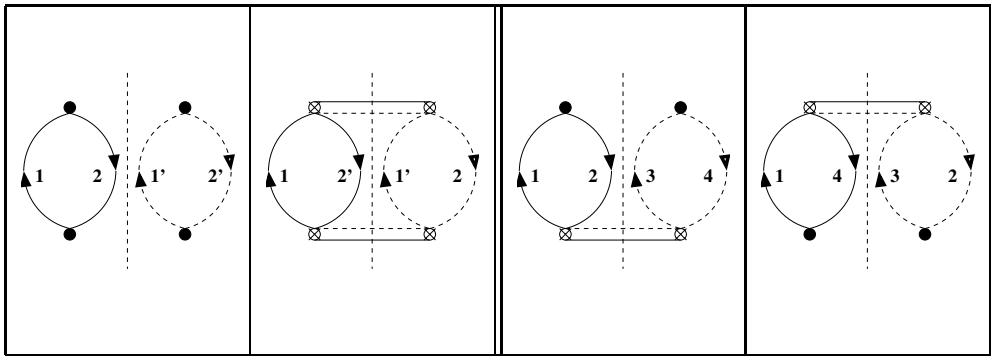

Figure 2. Processes x_1x_2, x_3x_4, x_5, x_6. The double (continuous and dashed) lines denote Andreev processes in both directions with incident electron and hole.

To calculate γ one must take into account all loops, which have at most one scattering event at each vertex at the S/F interfaces. The loops that must be taken into account and are not basic (like x_1x_2 and x_3x_4) have a sign, which is given by $(-1)^{\nu-1}$, where ν is the number of the basic loops from which they are made up ($\nu = 2$ for the above cases) [53].

2.2. *Josephson current*

The current will be calculated from the Green's function approach of Furusaki and Tsukada [59], which includes both the discrete spectrum and the continuum contributions. In Green's function we must sum over all possible $\vec{k}_\parallel$ values, so that

$$I = \frac{e}{2\hbar} k_B T \sum_{\vec{k}_\parallel} \sum_{\omega_n,\sigma} \frac{\Delta_L}{\Omega_{nL}} (k_{eL} + k_{hL}) \left(\frac{A_{eL,\sigma}}{k_{eL}} - \frac{A_{hL,\sigma}}{k_{hL}} \right), \tag{13}$$

where we sum over the Matsubara frequencies $\omega_n = (2n+1)\pi k_B T/\hbar$ for $n = 0, \pm 1, \pm 2, \ldots$ and the expression is evaluated using the analytic continuation $E + i0^+ \to i\hbar\omega_n$, so that $\Omega_L \to i\Omega_{nL}$. The formula takes into account the degeneracy between left-going electron and right-going hole and the same for the opposite directions, while there is also a summation over spins, since the exchange field splits the energy levels. In the following for simplicity we will omit the spin index, but we should keep in mind that many quantities that enter the Andreev amplitudes are spin dependent, with the electron and hole components of the quasiparticles corresponding to opposite spins. The quantities A_{eL} and A_{hL} are the Andreev amplitudes for electron and hole correspondingly incident from the left superconductor. While each Andreev amplitude is a complicated expression, the combination in (13) leads to cancellations from the two terms and great simplification in the numerator of this expression. The denominator is proportional to Γ, as defined earlier, taking into account the analytic continuation at the Matsubara frequencies:

$$\frac{A_{eL}}{k_{eL}} - \frac{A_{hL}}{k_{hL}} = \tilde{a}_{eR} \left(\tilde{c}_{hL} \frac{c^*_{eL}}{k_{eL}} - \tilde{d}_{hL} \frac{d^*_{hL}}{k_{hL}} \right) \frac{1}{\Gamma} + \tilde{a}_{hR} \left(\tilde{d}_{eL} \frac{d^*_{eL}}{k_{eL}} - \tilde{c}_{eL} \frac{c^*_{hL}}{k_{hL}} \right) \frac{1}{\Gamma}. \tag{14}$$

The terms that contribute in (14) to first order (proportional to a_{eR} or a_{hR}) are described by the diagrams in figure 3, if we neglect the expansion of Γ.

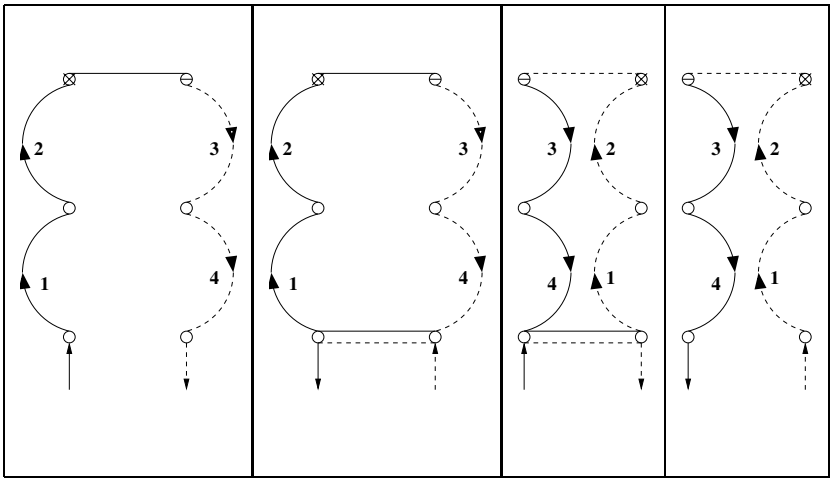

Figure 3. First-order processes that contribute to the current.

And finally using (13) and (14) the current is

$$I = \frac{e}{2\hbar} k_B T \sum_{\vec{k}_\parallel} \sum_{\omega_n,\sigma} \frac{\Delta_L}{\Omega_{nL}} (k_{eL} + k_{hL}) \frac{1}{\Gamma} \left[\tilde{a}_{eR} \left(\tilde{c}_{hL} \frac{c^*_{eL}}{k_{eL}} - \tilde{d}_{hL} \frac{d^*_{hL}}{k_{hL}} \right) + \tilde{a}_{hR} \left(\tilde{d}_{eL} \frac{d^*_{eL}}{k_{eL}} - \tilde{c}_{eL} \frac{c^*_{hL}}{k_{hL}} \right) \right], \tag{15}$$

where the starred quantities are for incidence from the superconductor side.

Finally combining (15) and the expressions in the appendix for the S_L/F interface parameters we find the expression

$$I = \frac{e}{2\hbar} k_B T \sum_{\vec{k}_\parallel} \sum_{\omega_n,\sigma} \frac{4D}{\Gamma \gamma_L \gamma_R} e^{i(q_e - q_h)d} \sin\phi, \tag{16}$$

with

$$D = -2(2iq_e)(2iq_h)(k_{eL} + k_{hL})(k_{eR} + k_{hR}) u_L v_L u_R v_R,$$

and all the quantities are expressed in the Matsubara frequencies with the analytic continuation $E + i0^+ \to i\hbar\omega_n$. Γ for the S/F/S structure is given by (11) and the γ_L and γ_R are the denominators in the scattering amplitudes given in the appendix (A.4).

3. Resonances for strong interface scattering

3.1. Single channel at normal incidence

To demonstrate the usefulness of the diagrammatic approach we consider the case of strong interface scattering in the double-barrier SIFIS junction. First we re-examine the 1D junction with $Z_L = Z_R = Z$ as a simple example. The case of strong interface potentials [52] means that the normal reflection processes are important, so that the denominator can be approximated by

$$\Gamma \approx 1 - x_1 - x_2 + x_1 x_2 = (1 - x_1)(1 - x_2),$$

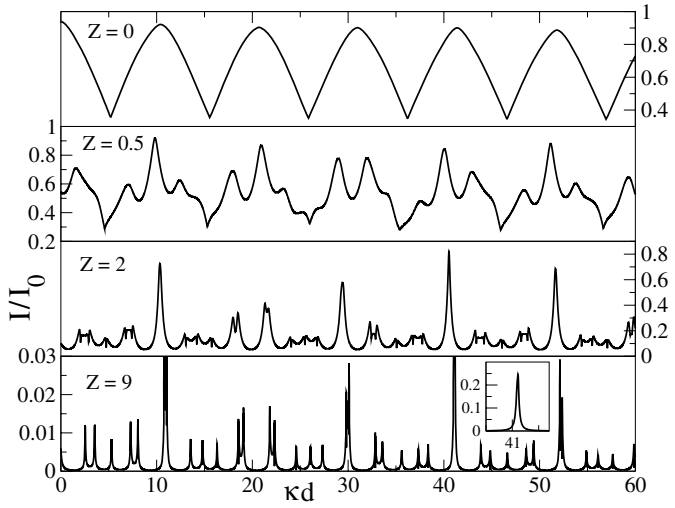

Figure 4. Normalized critical current versus κd for $h = 0.3$ and $Z = 0, 0.5, 2, 9$, from top to bottom. For $Z = 9$ the approximation $\Gamma \approx (1 - x_1)(1 - x_2)$ is indistinguishable in this scale. The inset in the bottom is for the peak around $\kappa d \approx 41$. $t = T/T_c = 0.1$.

and the resonances due to the double barrier will dominate the critical current. Thus in figure 4 we show the critical current (absolute value) as a function of the ferromagnet width (κd) for four different values of interface scattering, $Z = 0, 0.5, 2.0, 9.0$ at $h = 0.3$. We see a transition from the exchange field dominant behavior at $Z = 0$ to the normal resonance dominance for $Z = 9$. At low Z we see broad peaks, while at high Z (even at $z = 0.5$) we can distinguish closely spaced spin-up electron and hole (the electron from the $1 - x_1$ term with spin up, i.e. at $2S_{e\uparrow} - \beta_{e\uparrow R} - \beta_{e\uparrow L} = 2n_i\pi$, $n_i =$ integer) and spin-down hole and electron (hole from $1 - x_2$ with spin down, i.e. at $2S_{h\downarrow} - \beta_{h\downarrow R} - \beta_{h\downarrow L} = 2m_i\pi$, $m_i =$ integer) normal resonances near the Fermi energy. They involve the round-trip propagation phases $2S_{e\uparrow}$ or $2S_{h\downarrow}$ and the phase shifts on electron (hole) reflection from the right and left interfaces, $\beta_{p\sigma\alpha}(p = e, h; \alpha = L, R)$. Remark that in the above classification the resonances are labeled by a spin index, since the electron and hole resonances for the same spin are almost coincident (since $h \gg \Delta$) at the Fermi energy. But even for energies in the gap their displacement is very small compared to that for spins from the exchange field. Thus it is sufficient to characterize the resonance peaks with the spin. We should remark that the term electron (hole) resonance means that the electron (hole) amplitudes are dominant in the ferromagnetic layer, but of course both of them contribute equally to the current, in order to deliver pairs on the superconductor side.

Note that for high Z the interface reflection amplitudes go to -1 like $1/Z^2$, so that the reflection phases are $\beta_p \approx \pm\pi$, and the resonances occur at approximately $\kappa q_\uparrow d_{i\uparrow} = n_i\pi$, or $\kappa q_\downarrow d_{i\downarrow} = m_i\pi$ correspondingly for the ith spin-up or spin-down resonances. The splitting of different spin resonances depends on the strength of the exchange field. There is an 'envelope' which corresponds to the periodicity determined by $S_e - S_h \approx \pi$, while even for small Z you can see the formation of the resonances, which are only slightly shifted from the low-transparency case. For weak Z, the main effect is from the exchange field, but there is also a small effect on the period and a shift due to the interface scattering amplitude phases, which also vary with the width. Thus besides the phase-dependent terms, for increasing Z several processes must be included in Γ, such as x_1, x_2, x_1x_2, etc, which introduce the precursors of

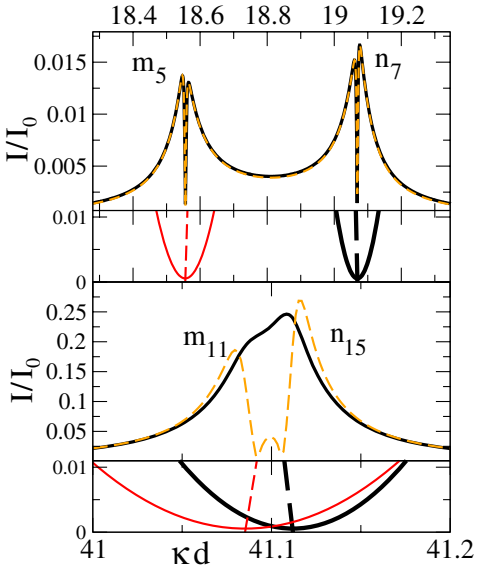

Figure 5. Blow up of figure 4 for $Z = 9$, near the resonant widths at (*a*) $\kappa d \approx 19$ and (*b*) $\kappa d \approx 41.1$. Solid curve is the result of the full diagrammatic contribution, while the approximation $\Gamma \approx (1 - x_1)(1 - x_2)$ is dashed line. Below each curve we plot $\Re$ (continuous) and $\Im$ (dashed) part of $(1 - x_{1,\uparrow})$ (thick lines) and $(1 - x_{2,\downarrow})$ (thin lines). The other parameters are the same as in figure 4.

the resonances. In fact even for $Z = 2$ one can observe the same resonances as for $Z = 9$, although slightly broader. Across each single-resonance peak (at high Z) there is a transition from 0- to π-junction [52], or vice versa. Starting from the low d part we can label the peaks (excluding those at $d = 0$) for example in the range $(0 < \kappa d < 20)$ consecutively as $n_1, m_1, n_2, m_2, n_3, n_4, m_3, n_5, m_4, n_6, m_5, n_7$, where n_i (m_i) corresponds to the spin-up (spin-down) resonance. Due to the difference of the electron (spin-up) and hole (spin-down) wave vectors at $E = 0$ in the ferromagnet, the resonances are split and they even cross each other at higher index resonances. Each spin resonance is split into two due to electron or hole resonances of the same spin, as seen in the blow up of two regions in figure 5.

To verify that the identification of spin-up (spin-down) electron or hole resonance is correct we blow up two regions for $Z = 9$ which include the large peak in the inset in the bottom of figure 4, near $d\kappa \approx 19$ and 41, in figure 5. First we discuss the peaks near $\kappa d \approx 19$, with $m = 5$ (left) and $n = 7$ (right). In the lower part (below each resonance) of the figure we plot separately $\Re(1 - x_{1,\uparrow})$ (thick continuous line), $\Im(1 - x_{1,\uparrow})$ (dark dashed) with spin up and $\Re(1 - x_{2,\downarrow})$ (thin continuous line), $\Im(1 - x_{2,\downarrow})$ (thin dashes) for spin down at $E = 0$ and we see for the case $(d\kappa \approx 19)$ sharp dips for the real part within 10^{-4} above zero at the minimum, at which the imaginary part also vanishes. Actually one can do even better and distinguish the electron and hole spin-down resonances by looking at the spectrum and finding the energies $(E < 0)$ that contribute at the two maxima of the spin-down $(m = 5)$ single resonance, with corresponding phases 0 and π. Thus each time a normal resonance (either electron or hole) approaches the Fermi level, we have the triggering of the transition and we get a structured double peak in the current [52], one of which corresponds to spin up (electron and hole) and the other to spin down (hole and electron). Thus we correctly identified the resonances as noted by the corresponding symbols. We also compared the full result with the

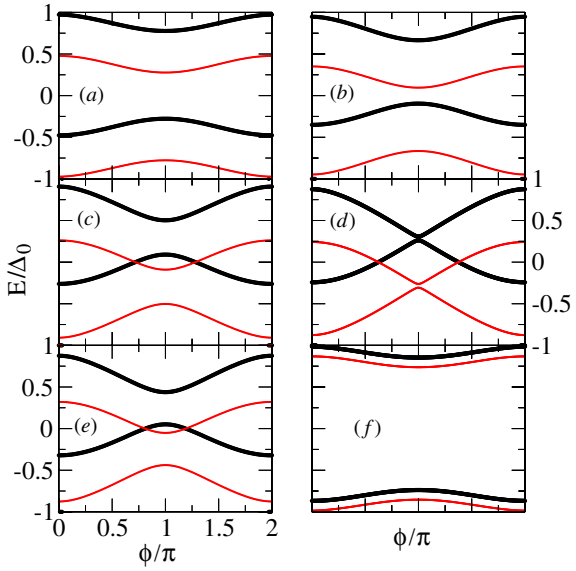

Figure 6. Andreev spectra for several widths for $Z = 9$, near the coincident resonance at $\kappa d =$ 41.07 (*a*), 41.08 (*b*), 41.09 (*c*), 41.099 (*d*), 41.11 (*e*), 41.15 (*f*). The other parameters are the same as in figure 4. The dark (gray) lines correspond to spin up (down) for the electron part.

approximation $\Gamma = 1 - x_1 - x_2 + x_1x_2 = (1 - x_1)(1 - x_2)$, and we saw that the two curves are indistinguishable within the scale of that figure. This seems to be the case, except near the strong peaks, where it is necessary to include the terms $-x_3 - x_4$ in the denominator, while the other terms (x_3x_4, x_5 and x_6) make no difference. In fact at the peak we have a sharp dip at the point of transition, while in the approximation (without x_3 and x_4) the transition is direct. To obtain the second harmonic contribution, which exists in the full denominator [32], the terms $-x_3 - x_4$ are necessary only near the transition and they do not influence the overall fitting of the critical current.

As d increases and after several pair resonances we can have almost coincidence of spin-up ($n = 15$) and down ($m = 11$) normal resonances (electron and hole) near $d\kappa \approx 41$, which leads to a significant increase of the maximum current. A prerequisite for the strong current at coincidence is the narrow resonances at high Z. In the highly expanded scale we can distinguish as before which is the spin-up (right) and spin-down (left) resonance. In this case the approximation $\Gamma = (1 - x_1)(1 - x_2)$ is not sufficient in the center, where both factors are small, so that it is necessary to include the Andreev terms $-(x_3 + x_4)$, and in that case the fitting is very good.

When we have coincidence of resonances then we remain in 0- or π-junction after the double resonance as well as at the peak. In fact to decide whether a region between peaks is 0 or π we need to count the electron and hole resonances before and the sign is $(-1)^{(n+m)}$. For example at $\kappa d = 20$ we have $n = 8$ and $m = 6$, so that we are in the zero phase. For the resonances shown on the top of figure 5 we have 0-junction in the left (since $n = 6, m = 4$), π-junction in the middle (since $n = 6, m = 5$) and in the right again 0-junction (since $n = 7, m = 5$). In the bottom figure in the left $n = 14, m = 10$ and in the right $n = 15, m = 11$ so that in both regions we are in 0-junction as well as in the center. If we look at the Andreev spectrum (figure 6) near the coincidence point we see that it has the 0-junction form, while at the center ($\kappa d \approx 41$) the spectrum gives the maximum

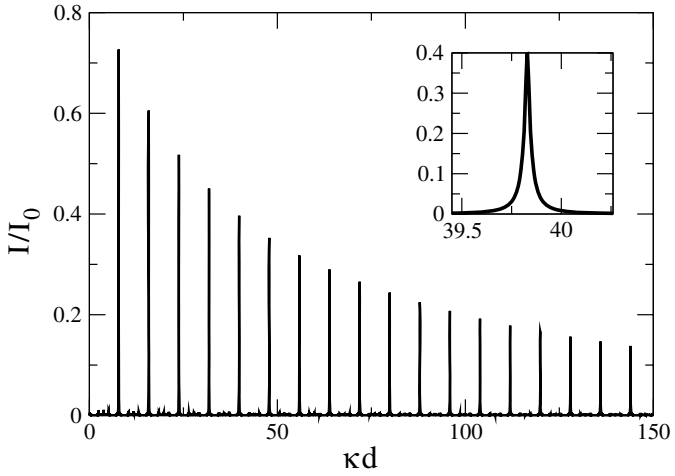

Figure 7. Normalized critical current versus κd for $Z = 9$ and $h = 0.3846$ obtained for $s = 3/2$. In the inset we blow up one of the resonances. The other parameters are chosen $t = T/T_c = 0.1$.

contribution to the current for both spin up and down at $\phi = \frac{\pi}{2}$. In fact the contribution almost approaches that with normal metal layer. Far from the peak the spectrum becomes flat, and the corresponding maximum current is quickly diminished. The closing up and reopening of the gap at $\phi = \pi$ for the branches with the same spin for the electron part is consistent with the increased transparency due to the double resonance. In fact for the low T considered the slopes of the ABS give the critical current. The spectrum is more usual at single resonances.

For strong Z where the resonances are sharp one can easily determine the approximate values of h and d for a given spin-up (n) and down (m) coincidence with ratio of integers $s = \frac{n}{m} > 1$ (for $0 < h < 1$), i.e.

$$h = \frac{1-s}{1+s}, \qquad \text{with} \quad \kappa d = \frac{n\pi}{\sqrt{1+h}}.$$

Thus in figure 7 we present the result for $s = 3/2$ and we see complete coincidence of all peaks, with indices multiples of 3 for spin up and multiples of 2 for spin down. The critical current amplitude decays with a dominant $\frac{1}{d}$. Note that this is also expected for normal ($h = 0$) layer, where resonances are spin independent ($s = 1/1$). The top of the narrow peaks needs the full-diagrammatic description. The minute peaks near the x-axis correspond to either up or down spin resonance. In the inset we see that through each coincident peak the junction preserves the phase, while for increasing width we have periodically 0- and π-phase, starting from π at the first peak, which is consistent with the following rule. For the $s = \frac{n}{m}$ case we have 0-phase for all coincidence peaks if $n - m =$ even. If $n - m =$ odd then we have the interchange of 0- and π-phase. The limit $s \to 1$ occurs for $h \to 0$ and gives the S/I/N/I/S limit.

3.2. 3d planar SIFIS junction

The question now is whether the strong peaks corresponding to the coalescence of resonances will survive in 3D, where we must integrate the effect of different incidence angles. Now the resonances occur at different angles and across a single resonance we have a sign change (due to a phase change of π) so that the integrated contribution around the resonant angle

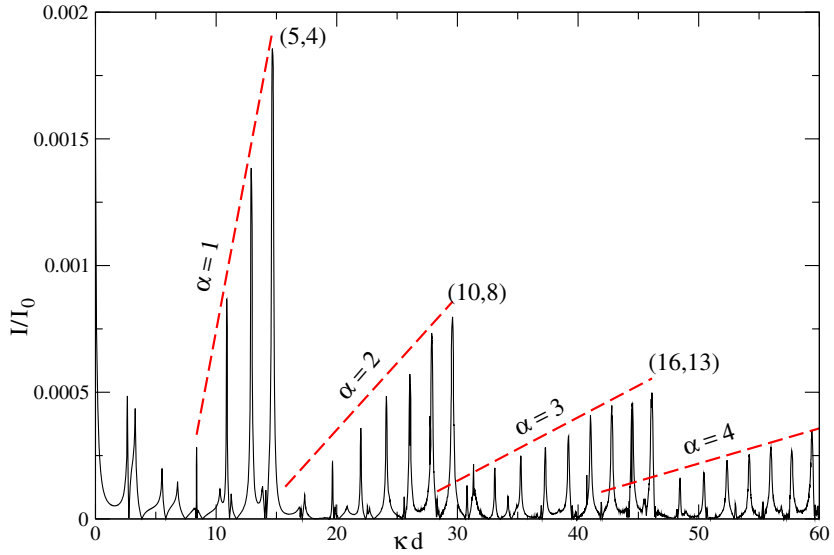

Figure 8. Normalized critical current versus κd for $Z = 9$ and $h = 0.2$ for a planar junction. The other parameters are chosen $t = T/T_c = 0.1$.

will tend to cancel out. This cancellation does not happen at normal incidence, as we saw in the single channel, where we have a significant contribution either positive or negative giving correspondingly 0- or π-junction. In the planar junction we have several single resonances at any width, but also coincident resonances are frequent. At coincidence we have no cancellation going through the resonance angle (due to 2π phase change) and the junction remains as 0- or π-junction with a significant current contribution. Also the contribution of the coincident resonances increases as the resonance incident angle approaches the normal incidence.

In figure 8 we plot the maximum current as a function of ferromagnet width for a low-transparency junction ($Z = 9$) and $h = 0.2$. What we see is an unexpected structure of overlapping grouped resonances. Most of the peaks arise from spin-up and spin-down resonance coincidence with different n and m indices of fixed $\alpha \equiv n - m = 1, 2, 3, \ldots$ for each group starting from the left. These resonances will be indicated by the pair (n, m) and occur at a finite incidence angle. The closer to the normal incidence the higher the peak in the current. Besides this we also have non-coincident spin-up or spin-down resonances, where either $1 - x_1$ (spin up) or $1 - x_2$ (spin down) vanishes at normal incidence. These are weaker and are more noticeable for small ferromagnet widths. Coincident resonances give a significant contribution in the angular integration and determine the peaked structure.

In figure 9 for the range $d\kappa = 0 - 10.0$ we see in sequence the n_1, m_1, n_2 and m_2 single resonances, which fall quite close to the prediction of the simple expressions of the previous section for the single channel. The sharp peak on the right ($\kappa d \approx 8.4$) is a (2, 1) coincidence. In the same figure, we plot the approximation by using only the x_1, x_2 and x_1x_2 terms and we see an excellent agreement almost everywhere except at the center of the (2, 1) peak. This is understandable since at the coincidence resonances both factors $1 - x_1$ and $1 - x_2$ vanish, so that the phase-dependent terms x_3, x_4 and the term x_3x_4 become important. So in the same figure we plotted the result with x_3 and x_4 included, but without the product x_3x_4, which

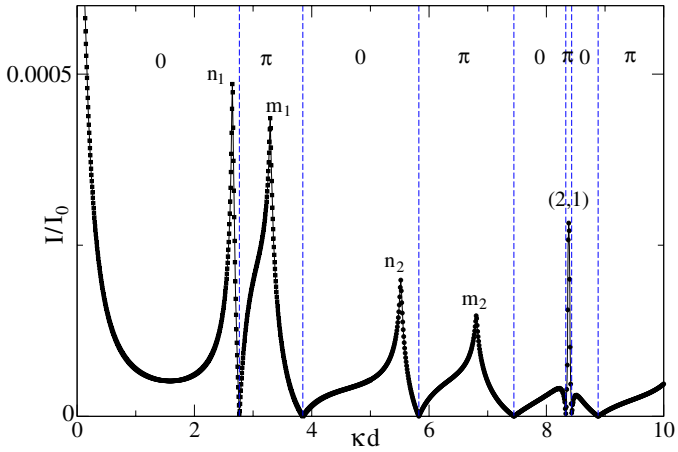

Figure 9. Normalized critical current versus κd for $Z = 9$ and $h = 0.2$ in the small-width region $d\kappa = 0 - 10.0$. The single resonances at normal incidence and the coincident resonance (2, 1) are identified. The regions of 0- or π-junction are indicated. The other parameters are chosen $t = T/T_c = 0.1$.

is much smaller. This curve is indistinguishable from the full summation of all closed-loop diagrams. Remark that on either side of the (2, 1) peak there appear two small peaks, which arise from the summation of the $n = 3$ single resonance with the strong and narrow (2, 1) coincidence resonance which has opposite current contribution. In the same figure we show the regions of 0- or π-junction and we see that between two single resonances we have a switch from 0 to π or vice versa. This can also be seen from the integrand as a function of the parameter $u = 1/\cos\theta$ for several widths shown in figure 10. The integrand includes the summation over the Matsubara frequencies and the indices $n(m)$ number the spin-up (down) resonances and the pair (n, m) the coincident resonances. Thus the current for a given width can have contributions of several resonances, but for each peak there is a dominant contribution which gives the label to the peak. If no coincident resonances or single resonances near normal incidence occur for strong Z the current is very small. Thus we see that at the widths of the first peak ($\kappa d = 2.67$) in the current (see figure 9) the contribution comes from the $n = 1$ (spin-up) resonance at normal incidence, while at the second peak ($\kappa d = 3.28$) the main contribution is from the $m = 1$ (spin down) at normal incidence while there is also a weak contribution from the $n = 1$ at a finite incident angle, with the former giving the main (positive) contribution and the label to the corresponding peak in the critical current, which is a π-junction. In (c) the main contribution comes from the $n = 2$ normal incidence resonance. In (e) clearly the coincident resonance dominates, while in (d) and (f), at the peaks on the either side, we see the competition between $n = 3$ (edging in) and the close resonances that coalesce to (2, 1).

In figure 11, we display the range of coincident spin-up and down resonances with $\alpha = n - m = 1$. We can clearly identify all the peaks in that family ordered in strength

$$(5, 4), (4, 3), (3, 2), (2, 1),$$

while for the absent $(6, 5)$ we have $u < 1$, i.e. imaginary angle of incidence. All four peaks correspond to π-junction. In the same figure we plot the approximation with $\Gamma = (1 - x_1)(1 - x_2)$ (dot-dash line), and we see that the fit is excellent everywhere except for the center of the coincidence peaks. So we added the terms x_3 and x_4 (but not the term x_3x_4 and

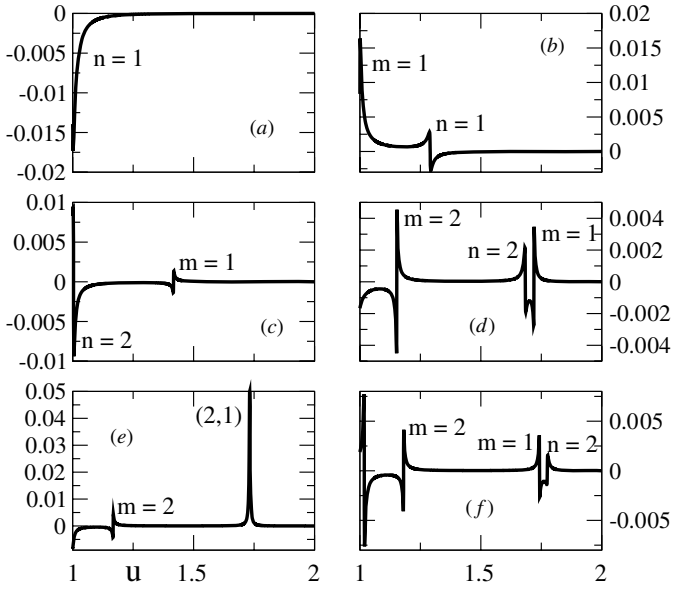

Figure 10. The integrand in the critical current as a function of incidence angle for several κd values for $Z = 9$ and $h = 0.2$. (*a*) $\kappa d = 2.67$, (*b*) $\kappa d = 3.28$, (*c*) $\kappa d = 5.51$, (*d*) $\kappa d = 8.2235$, (*e*) $\kappa d = 8.370$ and (*f*) $\kappa d = 8.503$. The other parameters are chosen $t = T/T_c = 0.1$.

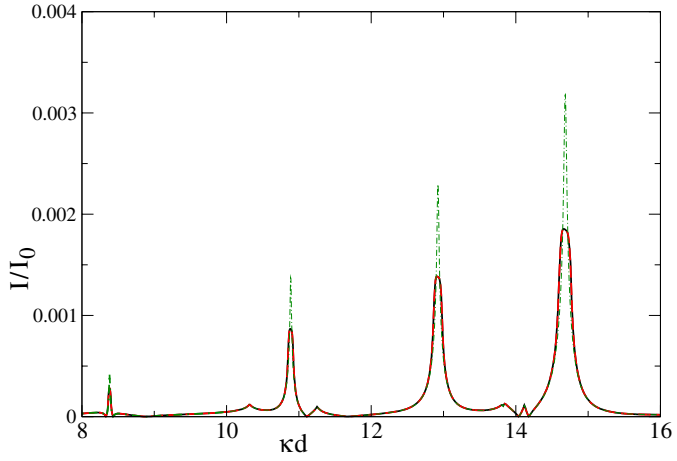

Figure 11. Normalized critical current versus κd for $Z = 9$ and $h = 0.2$ in the width region $\kappa d = 8.0$–16.0 that covers the family $\alpha = 1$ coincident resonances. The continuous line is the result of the full diagrammatic summation, while the dot-dashed line uses the approximation $\Gamma = (1 - x_1)(1 - x_2)$ and the dashed line includes the terms x_3 and x_4 and coincides with the full result. $t = T/T_c = 0.1$.

also omitting the other terms), and the result is indistinguishable from the full denominator. In the same figure we see the single resonances m_3, n_4 on either side of (3, 2). On the left side of (5,4) we see the (3, 1), which belongs to the family $\alpha = 2$. Close by and further to the left we have the m_4, while the n_5 is also hidden there, since it is much weaker.

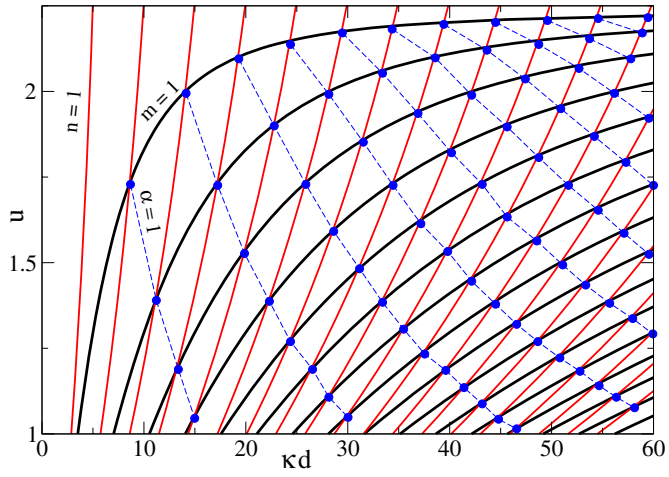

Figure 12. Plot of $u = 1/\cos\theta$ versus width κd for the single spin-up (light line) and spin-down (dark line) resonances labeled from left to right. At their intersection we see the angles of coincident resonances, while the intersections with the horizontal axis are the single or coincident resonances at normal incidence. The dashed lines are drawn by hand and connect resonances in the same family. $Z = 9$, $h = 0.2$ and $t = T/T_c = 0.1$.

Returning to figure 8, in each α family the highest peak occurs at near normal incidence and for decreasing amplitude (to the left) it occurs toward parallel to the surface incidence. The families are overlapping to the left. All the peaks can be accounted by simple expressions. If we use the variable $u = 1/\cos\theta$ and the ratio of spin-up to spin-down indices $s = \frac{n}{m}$, we have from the resonant conditions that at the (n, m) coincidence,

$$u = \sqrt{\frac{s^2 - 1}{s^2 + 1}\frac{1}{h}}, \qquad \kappa d = m\pi\sqrt{\frac{s^2 - 1}{2h}}, \qquad s = \frac{n}{m} \geqslant 1, \quad 1 \leqslant u.$$

In the second family $\alpha = 2$ we see the peaks

$$(10, 8), (9, 7), (8, 6), (7, 5), (6, 4), (5, 3), (4, 2), (3, 1)$$

the last of which is weak (but still can be noticed to the left of the (5,4) peak and mixed with the $m = 4$ single resonance. In the next family $\alpha = 3$, all the main peaks starting from the $(16, 13)$ down to $(4, 1)$ can be seen with little effort. Of course, there are other small peaks which come from higher families or from higher single resonances. Part of the family $\alpha = 4$ is also shown. The labeling of the resonances is facilitated by the resonance diagram in figure 12. There we can see for a given width at what incidence angle we have single and coincident resonances. The spin-up resonances are shown by the light lines labeled by n from the left and the spin-down resonances by the continuous lines labeled by m, while their intersections give the coincident resonances,

$$\kappa d_n\sqrt{\frac{1}{u^2} + h} = n\pi, \qquad \kappa d_m\sqrt{\frac{1}{u^2} - h} = m\pi.$$

The long dashed lines are drawn by hand and connect the families of coincident resonances for $\alpha = 1, 2, 3, 4, 5, 6\ldots$. Actually one can get simple expression for each α. From the diagram one can also determine the sign of the contribution to the current over angle regions, if one starts from the corner at $d = 0$. The rules are simple and work as seen from a careful analysis.

- Every time you cross vertically a single resonance line the contribution to the current changes sign, while it has the same sign when you pass a coincident point.
- The sign is the same for all points within a single rhombic region surrounded by the resonance lines $n, n+1, m, m+1$.
- The sign of the current can be determined by the dominant contribution which is the coincident points (near widths where they exist) whose strength decreases as we go away from normal incidence and as we move from one family to another with higher α.
- There is also a decrease for the single resonances for increasing widths.

Thus one can see that the $(2, 1)$ and the $n = 3$ contribute to the same widths, and similarly there is an overlap around the $(5, 4)$, m_4 and n_5. These and many other features in the maximum current can be explained by looking at the diagram in figure 12 and applying the above rules.

4. Summary

In this paper we considered the ballistic limit for the low-transparency double-barrier ferromagnetic S/I/F/I/S structure, both for the single-channel case and the 3D junction where we must take into account all the possible incidence angles. We used the diagramatic approach for the denominator of the Andreev amplitudes which includes all the closed paths in the internal ferromagnetic layer between the strong barriers. We use the scattering amplitudes for each interface. The approach gives the possibility to decide which are the dominant paths, which helps both to speed up the calculations and gain insight into the resonance structure. The current is calculated using the Green's function approach in terms of the Andreev reflection amplitude and the expression for the current is simplified using the diagramatic procedure.

For normal incidence we find the possibility of strong coincident resonances which can be much stronger than the usual spin-up or spin-down resonances, which are Zeemann split due to the exchange field. Remark that for $h = 0$ the spin-up and spin-down resonances are coincident and only slightly different for electron and hole. This splitting is still present here (see figure 5) and between them we have the 0- to π transition. As you increase the width of the junction from the phase build up you can have different order spin up or down coincide. In fact one can choose the exchange field so that all the resonances that satisfy the ratio $s = \frac{n}{m}$ coincide with a strong enhancement of the critical current in this case. We saw that away from the resonances the approximation of the denominator $\Gamma \approx (1 - x_1)(1 - x_2)$ is sufficient, while on the resonance we need to also include the term $-(x_3 + x_4)$. Still however we omit three other terms. Thus we have an efficient way to obtain the Andreev spectrum and the current. The approach can also consider band mismatch (Fermi energy, etc besides the exchange field) and the relevant information is included in the interface scattering amplitudes.

The next step was the 3D case where one might think that due to the contribution of many angles the resonances might wash away. To our surprise they are still there. Not only they are well identified but also they have some structure. Again we have single resonances at normal incidence which contribute to the current and at finite angles, whose contribution almost cancels out. The picture is dominated by *coincident resonances* at finite angles, because here the current keeps the same sign across the double resonance. Also in 3D one can choose the exchange field so that the coincidences occur at normal incidence with greatly increased amplitude.

These resonances can also be seen in the case where the left and right superconductors or the barriers are different. The same is true in the case of misfit (energy or mass). In the first case we also expect some broadening of the resonances.

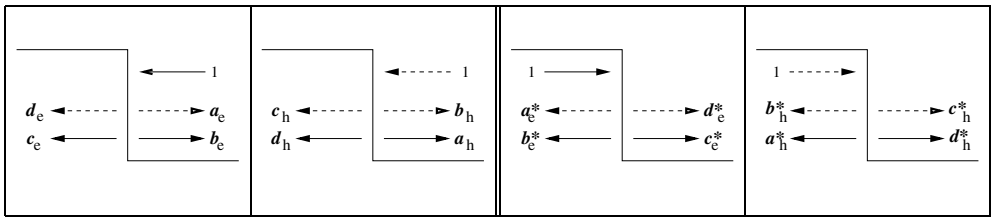

Figure 13. Definition of the scattering amplitudes at the left S/F interface. The same holds for the right S/F interface, with the starred amplitudes again corresponding for incidence from the superconductor side.

These resonances could be observable for clean junctions and strong insulating barriers which are uniform in thickness [17]. Even for weaker interface scattering the resonant features can be detected. Thus most of the features are seen for $Z = 4$ except that the peaks are slightly broadened. The numerical results show that some small nonuniformity can be tolerated before resonances strongly overlap. To minimize nonuniformity one can also think instead of infinite and narrow barriers the possibility of finite width and height barriers.

Appendix. Scattering amplitudes of the S/F interface

The analytical expressions for the scattering amplitudes from the S/F interfaces are given below (see figure 13). We use the convention that the unstarred elements are for incidence from the ferromagnet side and the starred (nothing to do with complex conjugation) from the superconductor side. The two superconductors are indexed with $\alpha = L, R$ and the corresponding neighboring ferromagnet with $i = 1, n$, in the case of n-ferromagnetic layers. The Andreev ($a_{p\alpha}$) and normal reflection ($b_{p\alpha}$) amplitudes for $p = e, h$-particle incidence from the ferromagnet side are

$$a_{p\alpha} = \frac{2(k_{e\alpha} + k_{h\alpha})q_{pi}u_\alpha v_\alpha}{\gamma_\alpha} e^{\mp i\phi_\alpha} \equiv a_{0p\alpha} e^{\mp i\phi_\alpha}, \qquad \text{for} \quad p = e, h, \tag{A.1}$$

where in the exponential $e^{\mp i\phi_\alpha}$, the sign is '$-$' (+) for incident electron (hole), with $\phi_\alpha = \mp\phi/2$ ($\alpha = L, R$),

$$b_{e\alpha} = -\frac{(k_{h\alpha} + q_{hi} - iZ_\alpha)(k_{e\alpha} - q_{ei} + iZ_\alpha)u_\alpha^2 - (k_{e\alpha} - q_{hi} + iZ_\alpha)(k_{h\alpha} + q_{ei} - iZ_\alpha)v_\alpha^2}{\gamma_\alpha}, \tag{A.2}$$

$$b_{h\alpha} = -\frac{(k_{h\alpha} - q_{hi} - iZ_\alpha)(k_{e\alpha} + q_{ei} + iZ_\alpha)u_\alpha^2 - (k_{e\alpha} + q_{hi} + iZ_\alpha)(k_{h\alpha} - q_{ei} - iZ_\alpha)v_\alpha^2}{\gamma_\alpha}, \tag{A.3}$$

where we omitted the spin index from the wave vectors, but we should keep in mind that the electron and the hole have opposite spins, and the amplitudes depend on the spin. The denominator is given by

$$\gamma_\alpha = (k_{h\alpha} + q_{hi} - iZ_\alpha)(k_{e\alpha} + q_{ei} + iZ_\alpha)u_\alpha^2 - (k_{e\alpha} - q_{hi} + iZ_\alpha)(k_{h\alpha} - q_{ei} - iZ_\alpha)v_\alpha^2. \tag{A.4}$$

Furthermore we need the normal ($c_{p\alpha}$) and branch crossing ($d_{p\alpha}$) transmission amplitudes. They are

$$c_{p\alpha} = \frac{2q_{pi}u_\alpha(k_{\bar{p}\alpha} + q_{\bar{p}i} \mp \mathrm{i}Z_\alpha)}{\gamma_\alpha} \mathrm{e}^{\mp \mathrm{i}\phi_\alpha/2}, \tag{A.5}$$

$$d_{p\alpha} = \frac{2q_{pi}v_\alpha(k_{p\alpha} - q_{\bar{p}i} \pm \mathrm{i}Z_\alpha)}{\gamma_\alpha} \mathrm{e}^{\mp \mathrm{i}\phi_\alpha/2}. \tag{A.6}$$

Finally, the starred coefficients for incidence from the superconductor side are

$$a^*_{p\alpha} = \frac{-2(q_{ei} + q_{hi})k_{p\alpha}u_\alpha v_\alpha}{\gamma_\alpha}, \tag{A.7}$$

$$b^*_{e\alpha} = \frac{(k_{h\alpha} + q_{hi} - \mathrm{i}Z_\alpha)(k_{e\alpha} - q_{ei} - \mathrm{i}Z_\alpha)u_\alpha^2 - (k_{e\alpha} + q_{hi} - \mathrm{i}Z_\alpha)(k_{h\alpha} - q_{ei} - \mathrm{i}Z_\alpha)v_\alpha^2}{\gamma_\alpha}, \tag{A.8}$$

$$b^*_{h\alpha} = \frac{(k_{h\alpha} - q_{hi} + \mathrm{i}Z_\alpha)(k_{e\alpha} + q_{ei} + \mathrm{i}Z_\alpha)u_\alpha^2 - (k_{e\alpha} - q_{hi} + \mathrm{i}Z_\alpha)(k_{h\alpha} + q_{ei} + \mathrm{i}Z_\alpha)v_\alpha^2}{\gamma_\alpha}, \tag{A.9}$$

$$c^*_{p\alpha} = \frac{2k_{p\alpha}u_\alpha\left(u_\alpha^2 - v_\alpha^2\right)(k_{\bar{p}\alpha} + q_{\bar{p}i} \mp \mathrm{i}Z_\alpha)}{\gamma_\alpha} \mathrm{e}^{\pm \mathrm{i}\phi_\alpha/2}, \tag{A.10}$$

$$d^*_{p\alpha} = \frac{2k_{p\alpha}v_\alpha\left(u_\alpha^2 - v_\alpha^2\right)(k_{\bar{p}\alpha} - q_{pi} \mp \mathrm{i}Z_\alpha)}{\gamma_\alpha} \mathrm{e}^{\mp \mathrm{i}\phi_\alpha/2}. \tag{A.11}$$

References

[1] Andreev A F 1964 *Sov. Phys.—JETP* **19** 1228
[2] Blonder G E, Tinkham M and Klapwijk T M 1983 *Phys. Rev.* B **25** 4515
[3] Beenaker C W J 1991 *Phys. Rev. Lett.* **67** 3836
[4] Furusaki A and Tsukada M 1991 *Phys. Rev.* B **43** 10164
[5] Halterman K and Valls O T 2004 *Phys. Rev.* B **70** 104516
Halterman K and Valls O T 2004 *Phys. Rev.* B **69** 014517
[6] Bagwell P F 1992 *Phys. Rev.* B **46** 12573
[7] Shumeiko V S and Bratus E N 1997 *Low Temp. Phys.* **23** 181
[8] Bulaevskii L N, Kuzii V V and Sobyanin A A 1977 *JETP Lett.* **25** 290
[9] de Jong M J M and Beenaker C W J 1995 *Phys. Rev. Lett.* **74** 1657
[10] Buzdin A 2000 *Phys. Rev.* B **62** 11377
[11] Buzdin A I 2005 *Rev. Mod. Phys.* **77** 935
[12] Golubov A G, Kupriyanov M Yu and Llichev E 2004 *Rev. Mod. Phys.* **76** 411
[13] Lyuksyutov I F and Pokrovsky V L 2005 *Adv. Phys.* **54** 67
[14] Zutic I, Fabian J and Sarma S Das 2004 *Rev. Mod. Phys.* **76** 323
[15] Bozovic I 2001 *IEEE Trans. Appl. Supercond.* **11** 2886
[16] Bozovic I, Lagvenov G, Verhoeven M A J, Caputo P, Goldobin E and Geballe T H 2003 *Nature* **422** 873
[17] Piano S 2008 arXiv:0807.0849v1 [cond-mat]
[18] Halterman K and Valls O T 2002 *Phys. Rev.* B **66** 224516
[19] Radovic Z, Lazarides N and Flytzanis N 2003 *Phys. Rev.* B **68** 014501
[20] Buzdin A I, Bulaevskii L N and Paniukov S V 1982 *JETP Lett.* **35** 178
[21] Radovic Z, Ledvij M, Dobrosarijevic-Grujic L, Buzdin A I and Clem J R 1991 *Phys. Rev.* B **44** 759
[22] Bergeret F S, Volkov A F and Evetov K B 2007 *Phys. Rev.* B **75** 184510
[23] Veretennikov A V, Ryazanov V V, Oboznov V A, Rusanov A Yu, Larkin V and Aarts J 2000 *Physica* B **284–8** 495
[24] Ryazanov V V, Oboznov V A, Rusanov A Yu, Veretennikov A V, Golubov A A and Aarts J 2001 *Phys. Rev. Lett.* **86** 2427
[25] Kontos T, Aprili M, Lesueur J, Genet F, Stephanidis B and Brursier R 2002 *Phys. Rev. Lett.* **89** 173007
[26] Sellier H, Baraduc C, Lefloch F and Calemczuk R 2003 *Phys. Rev.* B **68** 054531
[27] Blum Y, Tsukernik A, Karpoviski M and Palevski A 2002 *Phys. Rev. Lett.* **89** 187004
[28] Bell C, Loloee R, Burnell G and Blamire M G 2005 *Phys. Rev.* B **71** 180501

[29] Piano S, Robinson J W A, Burnell G and Blamire M G 2007 *Eur. Phys. J.* B **58** 123
[30] Robinson J W A, Piano S, Burnell G, Bell C and Blamire M G 2006 *Phys. Rev. Lett.* **97** 177003
[31] Kontos T, Aprili M, Lesueur J and Grison X 2001 *Phys. Rev. Lett.* **86** 304
[32] Sellier H, Baraduc C, Lefloch F and Calemczuk R 2004 *Phys. Rev. Lett.* **92** 257005
[33] Bergeret F S, Volkov A F and Evetov K B 2001 *Phys. Rev.* B **64** 134506
[34] Chtchelkatchev N M, Belzig W, Nazarov Yu V and Bruder C 2001 *JETP Lett.* **74** 323
[35] Barash Yu S and Bobkova I V 2002 *Phys. Rev.* B **65** 144502
[36] Chtchelkatchev N M 2004 *JETP Lett.* **80** 743
[37] Mohammadkhani G and Zareyan M 2006 *Phys. Rev.* B **73** 134503
[38] Prinz G A 1995 *Phys. Today* **48** 58
[39] Wang Y, Lu Z-Y, Zhang X-G and Han X F 2006 *Phys. Rev. Lett.* **97** 087210
[40] Cayssol J and Montambaux G 2004 *Phys. Rev.* **70** 224520
[41] Kulik I O 1970 *Sov. Phys.—JETP* **30** 944
[42] Ishii C 1970 *Prog. Theor. Phys.* **44** 1525
[43] Cakir O and Kulik I O 2003 *Phys. Rev.* B **67** 174514
[44] Shafranjuk S E and Ketterson J B 2005 *Phys. Rev.* B **72** 024509
[45] Gogadge G A and Kosevich A M 1998 *Low Temp. Phys.* **24** 716
[46] Brinkman A and Golubov A A 2000 *Phys. Rev.* B **61** 11297
[47] Kuhn D D, Chtchelkatchev N M, Lesovic G B and Blatter G 2001 *Phys. Rev.* B **63** 054520
[48] Ciuhu C, Lodder A, Otadoy R E S and Koperdraad R T W 2003 *J. Phys.: Condens. Matter* **15** 1847
[49] Galaktionov A V and Zaikin A D 2002 *Phys. Rev.* **65** 184507
[50] Gogadge G A and Kosevich A 1998 *Low Temp. Phys.* **24** 540
[51] Wendin G and Shumeiko V S 1996 *Phys. Rev.* B **53** R6006
[52] Petkovic I, Chtchelkatchev N M and Radovic Z 2006 *Phys. Rev.* B **73** 184510
[53] Paltoglou V, Margaris I and Flytzanis N 2007 *J. Phys. A: Math. Theor.* **40** 1289
[54] Nevirkovets I P, Shafranjuk S E and Ketterson J B 2003 *Phys. Rev.* B **68** 024514
[55] Tang H X, Wang Z D and Zhang Y 1996 *Z. Phys.* B **101** 359
[56] Hurd M and Wendin G 1994 *Phys. Rev.* B **49** 15258
[57] Paltoglou V, Margaris I and Flytzanis N 2006 *J. Phys. A: Math. Gen.* **39** 1
[58] Paltoglou V, Margaris I and Flytzanis N 2007 *Int. J. Mod. Phys.* **21** 505
[59] Furusaki A and Tsukada M 1991 *Solid State Commun.* **78** 299